processes

MDPI

*Article*

# Simulation and Performance Evaluation of Trans-Critical $CO_2$ Refrigeration System Integrated with Spray-Cooled Gas Coolers

**Lei Chai *, Savvas A. Tassou and Konstantinos M. Tsamos**

Centre for Sustainable Energy Use in Food Chains (CSEF), College of Engineering, Design and Physical Sciences, Brunel University of London, Uxbridge UB8 3PH, UK; savvas.tassou@brunel.ac.uk (S.A.T.); ktsamos@halcor.com (K.M.T.)

* Correspondence: lei.chai@brunel.ac.uk; Tel.: +44-1895-265834

**Abstract**

Rising ambient temperatures pose significant challenges to the thermodynamic performance of trans-critical $CO_2$ refrigeration systems, as they reduce system efficiency and cooling capacity. To mitigate these adverse effects, a spray-cooling technique was employed to enhance the heat rejection process. A mathematical model of the spray-cooled gas cooler, employing a homogeneous-mixture assumption that treats air and water droplets as a single phase without velocity slip or temperature difference, was developed and validated against experimental data. The developed model was subsequently integrated into the refrigeration system model to evaluate the system's performance with an air temperature range of 30 °C to 40 °C. The results show that spray cooling effectively decreases the $CO_2$ pressure and temperature exiting the gas cooler, lowers the compressor power consumption, enhances the evaporator cooling capacity, and significantly improves the overall system performance. The results also indicate that increasing the spray-water-to-air-mass flow rate ratio beyond around 0.075 yields negligible gains. Under conditions of air temperature of 40 °C, air velocity of 2 m/s and spray-water temperature of 25 °C, the coefficient of performance increased from 1.53 to 2.74, the heat rejection rate rose by 9.8%, the cooling capacity improved by 33.3%, and the compressor power consumption decreased by 25.9% as the spray-water-to-air-mass flow rate ratio increased from 0.02 to 0.075.

**Keywords:** rising ambient temperatures; trans-critical $CO_2$ systems; thermodynamic analysis; spray cooling

## 1. Introduction

Carbon dioxide ($CO_2$) is a natural refrigerant with a low global warming potential and zero ozone depletion potential, which make it an environmentally sustainable alternative to synthetic refrigerants such as hydrofluorocarbons (HFCs) like R404A. $CO_2$ offers a high volumetric cooling capacity, which allows for the use of more compact system components, and exhibits favorable heat transfer characteristics that enhance gas cooler performance. $CO_2$-based systems can operate efficiently across a broad temperature range, which makes them suitable for both low- and medium-temperature applications [1]. Owing to these advantages, trans-critical $CO_2$ refrigeration systems have gained widespread deployment, including in supermarket refrigeration, industrial cooling, heat pumps, and air conditioning applications [2]. According to a recent ATMOsphere report, by the end of 2023, more than 68,500 food retail outlets in Europe had implemented trans-critical $CO_2$ systems, corresponding to a market penetration of 22.9%, up from 18.4% in 2022 [3]. This rapid



Academic Editor: Blaž Likozar

Received: 5 February 2026
Revised: 5 March 2026
Accepted: 9 March 2026
Published: 12 March 2026

growth has been driven by new store developments, supermarket retrofits, and regulatory initiatives such as the European Union's F-Gas Regulations. The European market for trans-critical $CO_2$ refrigeration systems was valued at approximately USD 25 billion in 2023 and is projected by Business Market Insights to expand to USD 71 billion by 2030 [4].

Driven by increasing greenhouse gas emissions and changes in land use, ambient temperatures have risen globally and regionally as a direct consequence of anthropogenic climate change. During the summer of 2024, the European Union experienced record-breaking heat, with surface air temperatures 1.54 °C above the 1991–2020 average [5]. In July 2024, several regions in southern Europe recorded peak temperatures exceeding 45 °C. These continuously rising ambient temperatures have a significant impact on the performance of trans-critical $CO_2$ refrigeration systems. As ambient temperatures increase, refrigeration systems must operate at higher pressures to maintain adequate heat rejection, which increases compressor power consumption and reduces system efficiency [6]. The higher ambient temperature also requires advanced control strategies capable of dynamically adjusting operating pressures to maintain high performance. Spray cooling is recognized as an effective method for heat transfer enhancement and temperature control, which has been widely used across diverse applications from electronics cooling to power generation [7]. This technique utilizes the evaporative cooling effect wherein fine water droplets are sprayed into the air stream before they enter the gas cooler [8]. As the droplets evaporate, the air temperature decreases and its relative humidity increases, thereby improving the heat rejection process. In trans-critical $CO_2$ refrigeration systems, finned-tube heat exchangers are commonly employed as gas coolers due to their compact structure and high thermal effectiveness [9]. When integrated with spray cooling, finned-tube gas coolers can offer additional advantages, as the fins promote uniform distribution of the cooling spray across the heat exchange surface [10]. The combination of spray cooling and finned-tube design facilitates rapid heat dissipation due to the enlarged effective surface area provided by the droplets and fins, resulting in more efficient cooling compared with conventional methods [11].

Numerous experimental and numerical studies have investigated the performance of spray cooling applied to finned-tube heat exchangers. Wataru et al. [12] examined the heat transfer and pressure drop characteristics of air/water mist flows across the banks of smooth tubes, micro-finned tubes, and finned tubes. Dreyer et al. [11] studied a four-pass finned-tube heat exchanger exposed to vertical air/water mist flow and showed a heat transfer enhancement of up to 3.5 times the dry condition performance. Walczyk [13] evaluated the heat transfer performance of an air-fin condenser with supplemental water spray and found a 125% increase in performance. Popli et al. [14] experimentally investigated a flat-tube louver-fin heat exchanger under both dry and wet conditions and reported substantial improvements in cooling capacity and emphasized the importance of effective surface wetting for compact flat-tube designs. Chen et al. [15] examined a flat aluminum microchannel heat exchanger under spray cooling and analyzed the effects of spray flow rate, airflow rate, and relative humidity. Their results indicated that excessive spray rates could block the airflow passages and diminish the heat transfer. Xiao et al. [10] studied a wavy finned flat-tube bundle subjected to spray cooling and found improved heat transfer with increasing air velocity and spray flow rate. Lee et al. [16] explored the heat transfer performance of falling spray films over horizontal circular tube arrays and analyzed the effects of water flow rate, tube position, and upward air velocity. Hasan and Sirén [17] compared the performance of plain and plate-finned circular tube heat exchangers under spray-cooling conditions and demonstrated a substantial heat transfer enhancement in plate-finned configurations. Wiksten et al. [18] and Ma et al. [19] developed mathematical models to describe heat and mass transfer, respectively, in wavy fin-and-tube heat

exchangers and staggered tube bundles under wet-surface conditions, and obtained the temperature distributions of humid air, liquid and water film, and relative humidity distribution of humid air. Jin et al. [20] experimentally investigated the performance of a spray-cooled plate-fin heat exchanger under various operating conditions and demonstrated that spray cooling can substantially reduce surface temperatures and increase heat transfer coefficients, particularly at moderate water-to-air ratios, and identified a plateau region where additional water offers negligible improvement. Bop et al. [21] numerically simulated the wetting behavior and heat transfer of water-sprayed finned-tube condensers and evaluated how spray angle, water flow rate, and ambient air velocity influence wet coverage and local cooling effectiveness. Zhu et al. [22] combined experimental testing and numerical simulations to evaluate spray-cooling performance on heat exchanger surfaces and investigated the influence of nozzle type, spray angle, water flow rate, and droplet distribution on heat transfer enhancement.

Despite extensive research on spray cooling, most studies have focused on water-based heat exchangers or conventional refrigerant condensers. There has been limited research on spray cooling applied to $CO_2$-based heat exchangers. The thermophysical properties of $CO_2$, particularly near the critical point, differ significantly from those of water or condensing refrigerant, so findings from them may not be directly transferable to the design and optimization of $CO_2$ finned-tube gas coolers. Therefore, in the current study, a detailed mathematical model of spray-cooled $CO_2$ finned-tube gas coolers was developed and employed to evaluate the system's performance. The novelty of the present paper lies in the system-level integration and thermodynamic impact assessment of spray-cooled gas cooler for trans-critical $CO_2$ refrigeration cycles, which has been scarcely addressed in the literature. Unlike previous studies that primarily focus on local heat transfer enhancement under spray cooling, this work significantly investigates the spray-cooled gas cooler's performance, optimal high-side pressure controlling, compressor power consumption, liquid receiver behavior, and evaporator mass flow rate in a trans-critical $CO_2$ system. The findings from this study will be significant for expanding the applicability of $CO_2$-based refrigeration technologies in high-temperature regions and promoting sustainable cooling solutions.

## 2. Model Description

### *2.1. Trans-Critical $CO_2$ Refrigeration System*

Unlike traditional subcritical cycles, trans-critical $CO_2$ systems operate above the critical point of $CO_2$ (31.1 °C, 73.8 bar), where heat rejection occurs in a gas cooler rather than through condensation in a conventional condenser. A typical trans-critical $CO_2$ refrigeration system for supermarket application is shown in Figure 1, which operates at three distinct pressure levels. The red lines denote the high-pressure side of the system (80–120 bar), corresponding to the supercritical region and encompassing the compression and gas-cooling processes. The blue lines indicate the intermediate-pressure section (30–50 bar), including the flash gas bypass line and phase separation within the liquid receiver. The green lines represent the low-pressure side of the cycle (20–30 bar), comprising the evaporation process and the suction return flow to the compressor. The main components of the system include the compressor, gas cooler, intermediate-pressure control valve (IPCV), liquid receiver, low-pressure control valve (LPCV), evaporator, gas-bypass control valve (GBCV), and accumulator. The operating cycle proceeds as follows: The compressor raises the pressure and temperature of $CO_2$ to supercritical conditions. The high-pressure supercritical fluid then enters the gas cooler, where heat is rejected to the ambient environment without phase transition. Subsequently, the cooled supercritical $CO_2$ expands through the IPCV to the intermediate pressure level, producing a two-phase mixture. This mixture flows

into the liquid receiver, where vapor–liquid separation occurs. The separated liquid phase expands through the LPCV to the evaporating pressure and enters the evaporator, where it absorbs heat from the cooling load, completely vaporizes, and exits as superheated vapor. Meanwhile, the vapor fraction from the receiver expands through the GBCV to the low-pressure level and mixes with the evaporator outlet stream. The combined vapor then passes through the accumulator, which stabilizes suction conditions before returning to the compressor, thereby completing the cycle. This multi-pressure configuration enables stable operation over a broad range of ambient conditions and enhances cooling capacity and overall energy efficiency.

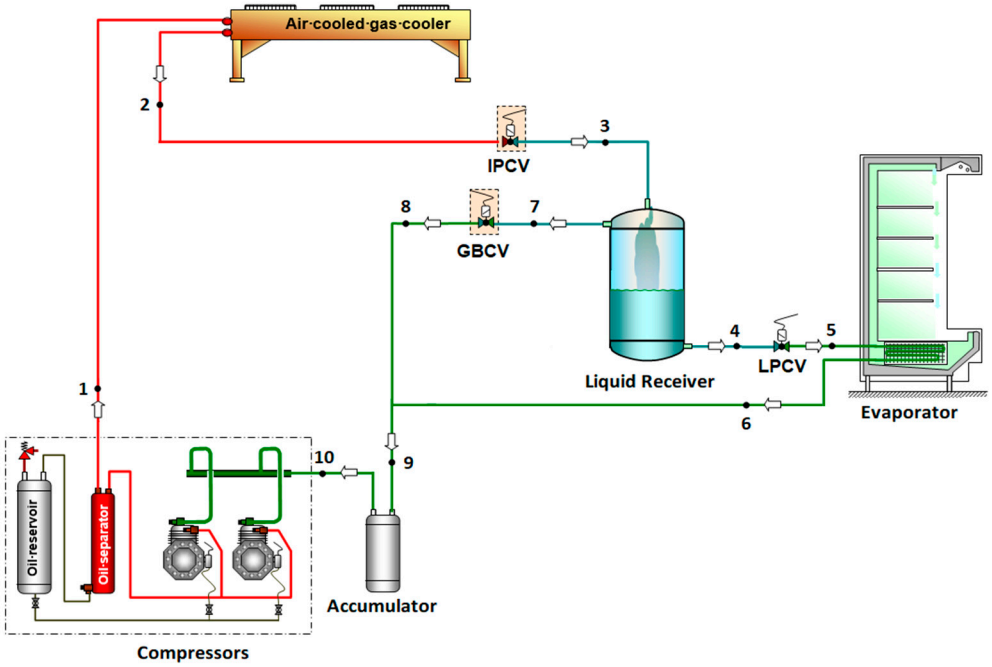


**Figure 1.** A typical trans-critical $CO_2$ refrigeration system for supermarket application.

### *2.2. Detailed Spray-Cooled Gas Cooler Model*

Given the sensitivity of gas cooler performance to air/water mixture temperature, a detailed mathematical model is crucial for accurately predicting heat transfer and pressure drop on both the $CO_2$ and air/water mixture sides. Figure 2 shows the distributed design for the gas cooler modeling. Each tube is evenly divided into $N$ segments along the $CO_2$ flow direction, and each segment is a crossflow heat transfer unit. The temperatures of $CO_2$ and air/water mixture for each segment are calculated by the $\varepsilon$–$NTU$ method of London and Seban [23]. The heat transfer rate from $CO_2$ to the air/water mixture is calculated as follows:

$$Q_i = \varepsilon_i C_{\min,i}(T_{CO2,i} - T_{mix,i}) \quad (1)$$

$$\varepsilon_i = \frac{1 - \exp\left[-NTU_i\left(1 - C_i^*\right)\right]}{1 - C_i^* \exp\left[-NTU_i\left(1 - C_i^*\right)\right]} \quad (2)$$

$$C_i^* = \frac{C_{\min,i}}{C_{\max,i}} \quad (3)$$

$$C_{\min,i} = \min\left(m_{mix,i} c_{pmix,i},\, m_{CO2,i} c_{pCO2,i}\right) \quad (4)$$

$$C_{\max,i} = \max\left(m_{mix,i} c_{pmix,i},\, m_{CO2,i} c_{pCO2,i}\right) \quad (5)$$

$$NTU_i = \frac{U_i A_i}{C_{\min,i}} \quad (6)$$

$$U_i A_i = \frac{1}{\frac{1}{h_{\mathrm{conv,CO2},i} A_{\mathrm{CO2},i}} + R_{\mathrm{t},i} + \frac{1}{h_{\mathrm{conv,mix},i} A_{\mathrm{mix},i} \eta_{\mathrm{mix},i}}} \tag{7}$$

where $Q$, $\varepsilon$, $C$, $NTU$ and $U$ represent heat transfer rate, heat exchanger effectiveness, capacity rate, number of transfer units and overall heat transfer coefficient, respectively. $T$, $m$, $h_{\mathrm{conv}}$, $A$ and $R_{\mathrm{t}}$ denote temperature, mass flow rate, heat transfer coefficient, heat transfer area and thermal resistance through the tube, respectively. $\eta$ represents the surface efficiency of a finned tube. $A_i$ is the total effective heat transfer area of segment $i$, $A_{\mathrm{CO2},i}$ is the internal heat transfer area on the $CO_2$ side of segment $i$, calculated as $A_{\mathrm{CO2},i} = \pi D_{\mathrm{i}}(L/N)$, and $A_{\mathrm{mix},i}$ is the external heat transfer area on the air/water mixture side of segment $i$, including both tube outer surface and fin surface contribution. The total mixture-side area is calculated from fin geometry using the equation $A_{\mathrm{total}} = A_{\mathrm{tube,ext}} + A_{\mathrm{fin}}$, and each segment area is calculated as $A_{\mathrm{mix},i} = A_{\mathrm{total}}/N$.

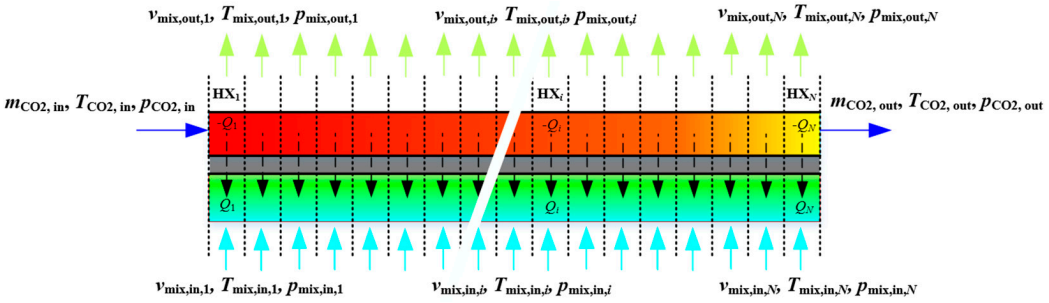


**Figure 2.** Distributed design for gas cooler modeling.

During model development, the air/water mixture entering the gas cooler is treated as a homogeneous continuum, assuming negligible velocity slip and thermal nonequilibrium between droplets and the carrier phase. Effective mixture properties, including density, specific heat capacity, thermal conductivity, and viscosity, are determined using phase-fraction-weighted averaging and applied directly in the governing equations of heat transfer and fluid flow. This assumption is particularly appropriate for finely atomized sprays with strong interphase momentum and heat transfer coupling, where relative motion and temperature gradients are minimal. This approach ensures computational tractability while retaining adequate accuracy for predicting convective heat transfer performance [24–26].

$$\rho_{\mathrm{mix}} = \frac{R_{\mathrm{wat-air}} + 1}{\frac{R_{\mathrm{wat-air}}}{\rho_{\mathrm{wat}}} + \frac{1}{\rho_{\mathrm{air}}}} \tag{8}$$

$$c_{p_{\mathrm{mix}}} = \frac{c_{p_{\mathrm{wat}}} R_{\mathrm{wat-air}} + c_{p_{\mathrm{air}}}}{R_{\mathrm{wat-air}} + 1} \tag{9}$$

$$k_{\mathrm{mix}} = \frac{k_{\mathrm{wat}} R_{\mathrm{wat-air}} + k_{\mathrm{air}}}{R_{\mathrm{wat-air}} + 1} \tag{10}$$

$$\mu_{\mathrm{mix}} = \frac{R_{\mathrm{wat-air}} + 1}{\frac{R_{\mathrm{wat-air}}}{\mu_{\mathrm{wat}}} + \frac{1}{\mu_{\mathrm{air}}}} \tag{11}$$

where $\rho$, $c_{\mathrm{p}}$, $k$ and $\mu$, respectively, are the density, specific heat, thermal conductivity and viscosity, and the subscripts mix, wat and air, respectively, denote the air/water mixture, spray water and air. $R_{\mathrm{wat\text{-}air}}$ is the spray-water-to-air-mass flow rate ratio ($m_{\mathrm{wat}}/m_{\mathrm{air}}$). The thermophysical properties of the homogeneous mixture are updated based on the local temperature and pressure of each segment.

The empirical correlations used to calculate heat transfer and pressure drop of $CO_2$, derived from Gnielinski [27] and Petukhov and Kirillov [28], are, respectively,

$$Nu_{CO2,\,i} = \frac{(f_{CO2,\,i}/8)(Re_{CO2,\,i} - 1000)Pr_{CO2,\,i}}{1 + 12.7\left(f_{CO2,\,i}/8\right)^{1/2}\left(Pr_{CO2,\,i}^{2/3} - 1\right)} \tag{12}$$

$$f_{CO2,\,i} = \left(0.790\ln Re_{CO2,\,i} - 1.64\right)^{-2} \tag{13}$$

where $Nu$, $f$, $Re$ and $Pr$ denote the Nusselt number, friction factor, Reynold number and Prandtl number, respectively. These correlations have been widely adopted in $CO_2$ gas cooler modeling studies due to their robustness and simplicity, particularly when combined with local property evaluation.

The air/water mixture heat transfer and pressure drop are determined by the correlations from Wang et al. [29].

$$j_{air,\,i} = \begin{cases} 0.9047 Re_{Dc,\,mix,\,i}^{j1}\left(\frac{F_s}{D_c}\right)^{j2}\left(\frac{P_t}{P_l}\right)^{j3}\left(\frac{S_s}{S_h}\right)^{-0.0305} N_r^{0.0782} & \text{for } N_r > 2 \text{ and } Re_{Dc,\,mix,\,i} < 700 \\ 1.0691 Re_{Dc,\,mix,\,i}^{j4}\left(\frac{F_s}{D_c}\right)^{j5}\left(\frac{S_s}{S_h}\right)^{j6} N_r^{j7} & \text{for } N_r = 1,\ 2 \text{ or } N_r > 2 \text{ and } Re_{Dc,\,mix,\,i} > 700 \end{cases} \tag{14}$$

$$f_{air,\,i} = 1.201 Re_{Dc,\,mix,\,i}^{f1}\left(\frac{F_s}{D_c}\right)^{f2}\left(\frac{P_t}{P_l}\right)^{f3}\left(\frac{S_s}{S_h}\right)^{f4} N_r^{f5} S_n^{f6} \tag{15}$$

where $j1$–$j7$, $f1$–$f7$ are correlation parameters referring to fin geometry; $F_s$, $D_c$, $P_t$, $P_l$, $S_s$, $S_h$, $N_r$, and $S_n$, respectively, refer to the fin spacing, fin collar outside diameter, transverse tube pitch, longitudinal tube pitch, slit breadth in the airflow direction, slit height, tube row number, and slit number in an enhanced zone. The thermal resistance through the tube is calculated as

$$R_{t,\,i} = \frac{1}{2\pi k_{tube}(L/N)} ln\left(\frac{D_o}{D_i}\right) \tag{16}$$

where $L$, $D_o$ and $D_i$ are the tube length and the outside and inside tube diameters, respectively.

In the development of the detailed spray-cooled gas cooler model, the inlet temperature and pressure of $CO_2$ are obtained from the upstream compressor discharge conditions. An initial estimate of the average outlet temperature of the air/water mixture is prescribed to define the boundary conditions for the gas cooler calculation. The modeling flow chart is shown in Figure 3. The inlet thermodynamic state of each segment is determined from the outlet conditions of the preceding one, ensuring energy and mass conservation and thermodynamic continuity throughout the calculation. The temperature of the cooling air/water mixture is updated after each tube row to capture the progressive heat absorption along the flow direction. Iterations are performed until convergence is achieved, defined by agreement between the calculated and prescribed inlet mixture temperature within an acceptable tolerance. The thermophysical properties of $CO_2$ are updated locally at each segment based on temperature and pressure to capture near-critical effects accurately.

To determine the inlet temperature of the air/water mixture to the gas cooler $T_{mix,in,0}$, a dedicated spray-cooling test facility was built at Brunel University of London. A low-flow-rate full-cone nozzle (WL1 90 from The Spray Nozzle People Group Ltd. at Upper Beeding, West Sussex, UK), illustrated in Figure 4, was installed 300 mm upstream of the tested finned-tube heat exchanger, which had an overall length of 560 mm, width of 351 mm and depth of 80 mm. The nozzle configuration and placement were selected to minimize flow maldistribution and ensure uniform droplet distribution, based on preliminary experimental observations. The mass flux of the evaporative spray water used for precooling the inlet ambient air (ambient temperature of 30 °C and relative humidity 50%

and spray-water temperature of 20 °C) can be quantified as a function of spray-water mass flux and ambient air-mass flux, derived from systematic experimental measurements.

$$G_{\mathrm{evap,wat}} = 0.10864G_{\mathrm{wat}} + 0.000662G_{\mathrm{air}} - 5.774 \quad (17)$$

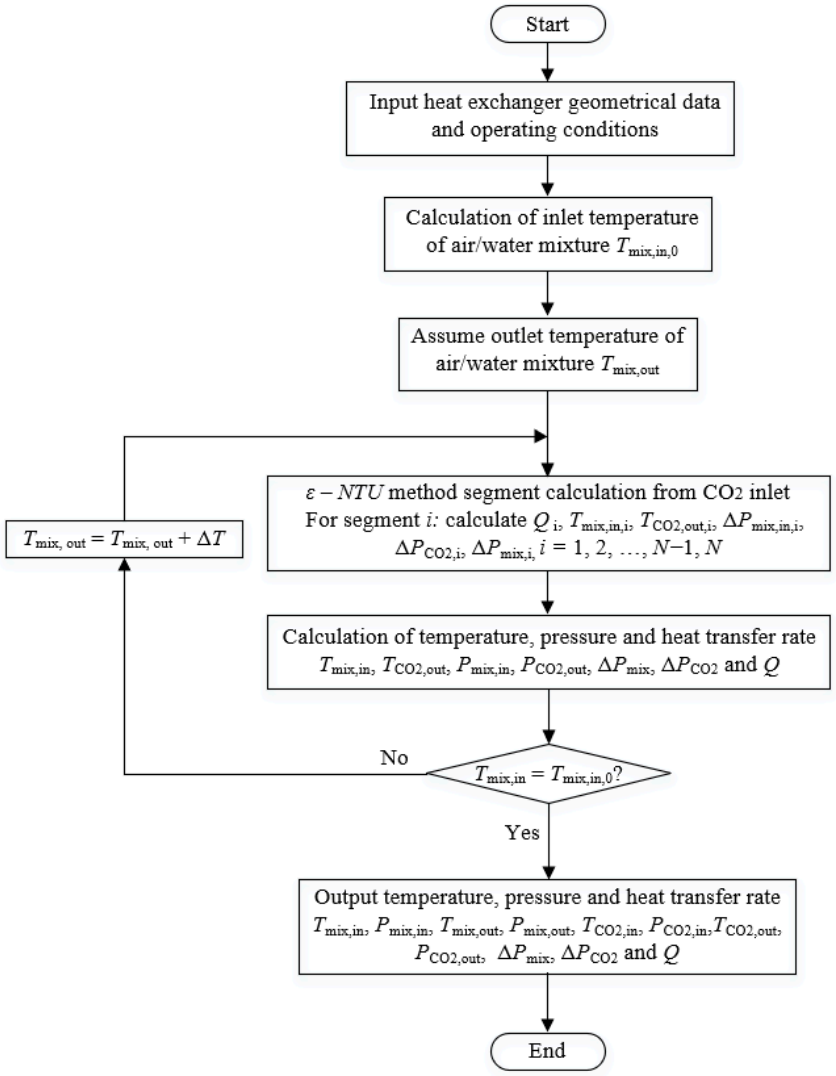


**Figure 3.** Flow chart of spray-cooled gas cooler modeling.

The mass fluxes of spray water, ambient air and air/water mixture are calculated from the spray area on the gas cooler and have the unit g × $m^{-2}$ × $s^{-1}$. The temperature of the air/water mixture entering the gas cooler can be calculated as:

$$T_{\mathrm{mix,in,0}} = \frac{m_{\mathrm{wat}} c_{p_{\mathrm{wat}}} T_{\mathrm{wat,in}} + m_{\mathrm{air}} c_{p_{\mathrm{air}}} T_{\mathrm{air,in}} - m_{\mathrm{evap,wat}} \Delta h_{\mathrm{wat,evap}}}{c_{p_{\mathrm{mix}}} (m_{\mathrm{wat}} + m_{\mathrm{air}})} \quad (18)$$

where $m_{\mathrm{evap,wat}}$ is the mass flow rate of the evaporative spray water and calculated from the mass flux and spray area. The intent of using this correlation was to accurately capture the inlet air temperature reduction, which is a critical boundary condition for gas cooler modeling. It should be noted that Equation (17) was derived under a specific nozzle configuration, airflow range, and installation distance; thus, its applicability is restricted to similar configurations and requires validation for different setups.

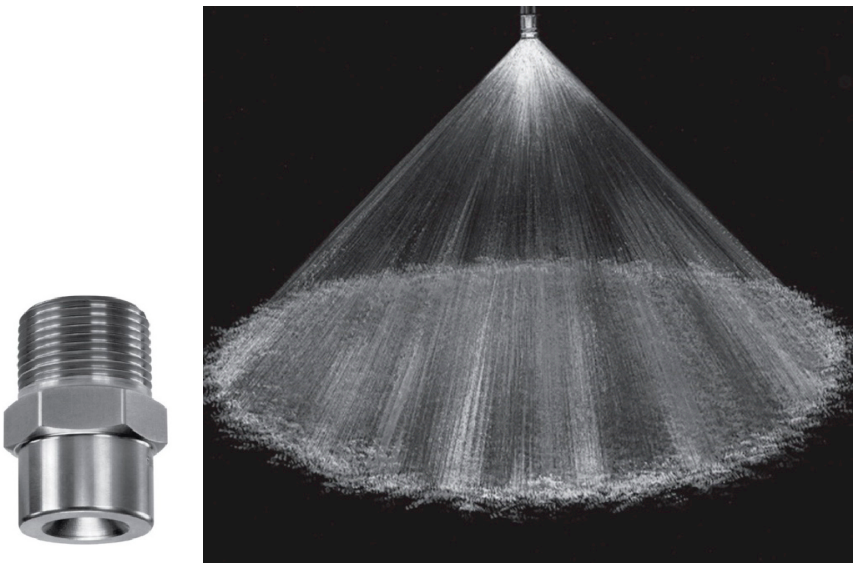

**Figure 4.** Full-cone nozzle (WL1 90) from The Spray Nozzle People Group Ltd.

### *2.3. $CO_2$ Refrigeration System Model*

In trans-critical $CO_2$ refrigeration systems, the high-side pressure critically influences system efficiency and overall performance. Because operation occurs above the critical point, the thermodynamic properties of $CO_2$ exhibit strong sensitivity to pressure and temperature variations. For a given ambient temperature, an optimal high-side pressure exists that maximizes system performance. The present analysis considers air temperatures ranging from 30 °C to 40 °C. For each air temperature, the high-side pressure is initially set to 75 bar and a pressure step of 0.1 bar. The coefficient of performance (*COP*) is calculated and subsequently evaluated over a defined pressure range. An iterative optimization procedure is implemented to identify the pressure corresponding to the maximum *COP*, which is defined as the optimal discharge pressure exiting the compressor. The system-level modeling framework is shown in Figure 5. For each discharge pressure, the calculation begins with an initial estimate of the compressor inlet temperature. Iterations are performed until the temperature obtained after completing a full refrigeration cycle converges to the assumed value, thereby ensuring thermodynamic consistency. The principal thermodynamic processes corresponding to Figure 1 are summarized in Table 1. The modelling code was written in the MATLAB R2023b programming language (The MathWorks Inc., Natick, MA, USA).

**Table 1.** Processes involved in the trans-critical $CO_2$ refrigeration system corresponding to Figure 1.

| No | Process |
|---|---|
| 10→1 | Non-isentropic compression in compressor |
| 1→2 | Heat rejection from $CO_2$ to air/water mixture in gas cooler |
| 2→3 | Isenthalpic expansion in IPCV |
| 3→4, 7 | Isenthalpic separation to liquid and vapor in liquid receiver |
| 4→5 | Isenthalpic expansion in LPCV |
| 5→6 | Heat absorption from the cooling load in evaporator |
| 7→8 | Isenthalpic expansion in GBCV |
| 6, 8→9 | Isenthalpic mixing process |
| 9→10 | Isenthalpic mixed flow |

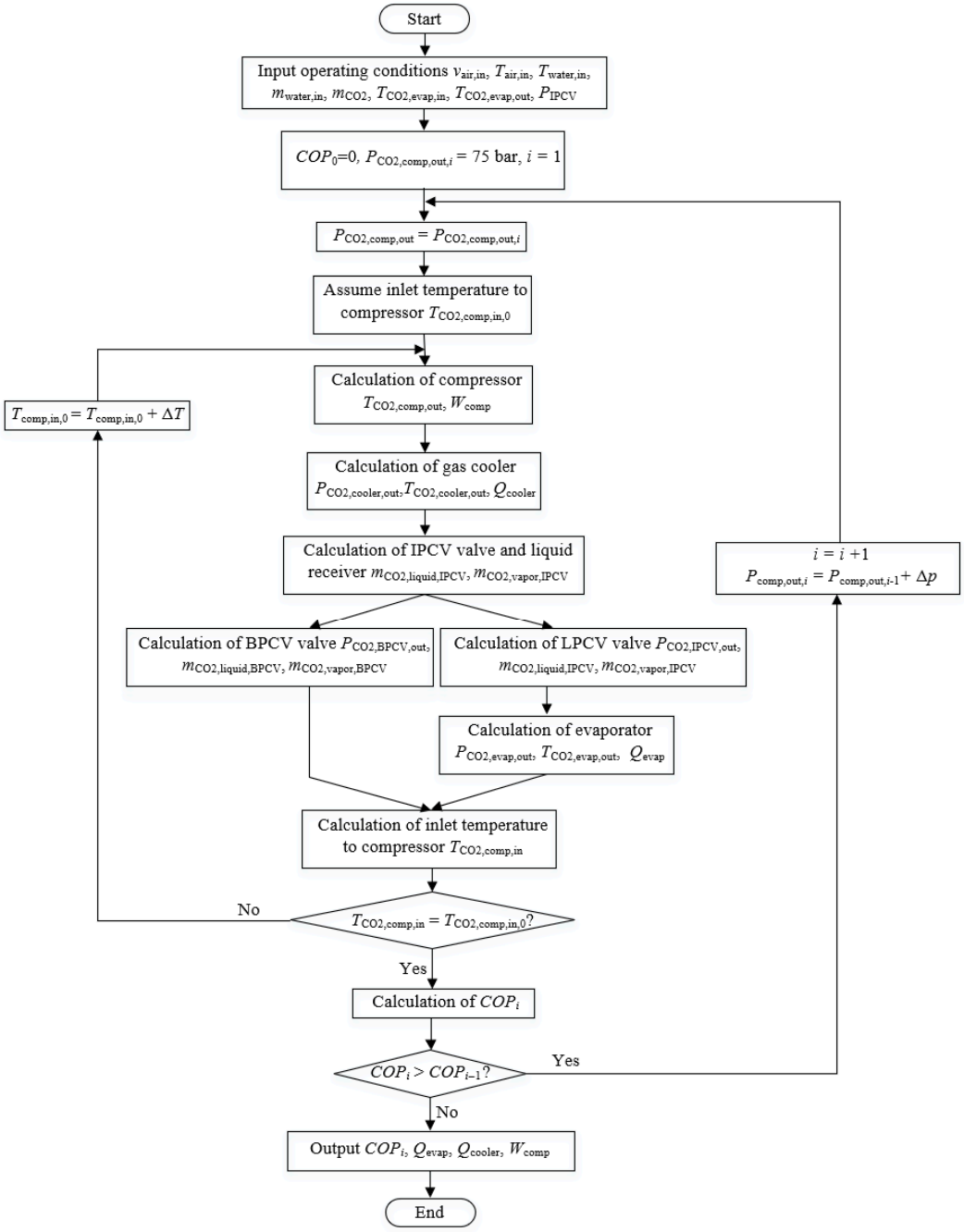


**Figure 5.** Flow chart of trans-critical $CO_2$ refrigeration system modeling.

For the system modeling, the compression process in the compressor is calculated from the isentropic efficiency ($\eta_{comp,is}$) obtained by Ge et al. [30].

$$\eta_{comp,is} = \frac{h_{comp,out,is} - h_{comp,in}}{h_{comp,out} - h_{comp,in}} \tag{19}$$

$$\eta_{comp,is} = 0.74443 - \frac{0.050539 P_{comp,out}}{P_{comp,in}} \tag{20}$$

$$W_{comp} = m_{CO2}\left(h_{comp,out} - h_{comp,in}\right) \tag{21}$$

where $h$ is the specific enthalpy, and $W_{comp}$ is the power consumption by the compressor. The specific enthalpies entering and exiting the compressor are calculated from the local temperature and pressure. The temperature and pressure exiting the gas cooler are de-

termined by the detailed model shown in Section 2.2. The specific enthalpy entering and exiting the gas cooler is also obtained from the local temperature and pressure.

$$Q_{\text{cooler}} = m_{\text{CO2}}(h_{\text{cooler,in}} - h_{\text{cooler,out}}) \tag{22}$$

where $Q_{\text{cooler}}$ is heat rejection rate from the gas cooler. The expansion processes through the IPCV, LPCV and GBCV are assumed to be isenthalpic throttling.

$$h_{\text{valve,out}} = h_{\text{valve,in}} \tag{23}$$

The $CO_2$ temperature after it has passed through the valves is obtained from the local pressure and specific enthalpy. The phase separation process in the liquid receiver and the mixing process in the accumulator are assumed to be isenthalpic.

$$h_{\text{rec,out}} = h_{\text{rec,in}} \tag{24}$$

$$x = \frac{h_{\text{rec,out}} - h_{\text{rec,out,liq}}}{h_{\text{rec,out,vap}} - h_{\text{rec,out,liq}}} \tag{25}$$

where $x$ is the mass quality of $CO_2$ in the liquid receiver. The cooling capacity of the evaporator is calculated from the obtained inlet temperature and mass quality of $CO_2$ after the LPCV and the assumed superheat at the outlet.

$$Q_{\text{evap}} = m_{\text{CO2}}(1 - x)\left(h_{\text{evap,out}} - h_{\text{evap,in}}\right) \tag{26}$$

The specific enthalpy exiting the evaporator is obtained from the local temperature and pressure. The evaporator model is intentionally simplified to isolate gas cooler effects. The specific enthalpy entering the compressor is calculated as follows:

$$h_{\text{comp,in}} = (1 - x)h_{\text{evap,out}} + xh_{\text{rec,out,vap}} \tag{27}$$

The temperature of $CO_2$ entering the compressor is a function of pressure and specific enthalpy. The present *COP* definition follows standard refrigeration practice and excludes auxiliary power consumption, such as spray-water pumps and fans. Given that power consumption by the compressor exceeds 2500 W, while it is <80 W by air fan and <10 W by spray-water pump, inclusion of auxiliaries slightly reduces *COP* but does not affect the qualitative performance improvement.

$$COP = \frac{Q_{\text{evap}}}{W_{\text{comp}}} \tag{28}$$

### *2.4. Modeling Assumption and Conditions*

During the modeling, the system is assumed to operate under steady-state conditions, with the intermediate pressure applied as the suction pressure for the LPCV. The heat losses to or from the surroundings are negligible, and the pressure losses in pipes and the evaporator are neglected.

The gas cooler is a 2-circuit finned-tube heat exchanger, previously employed by Santosa et al. [31] to investigate the air- and refrigerant-side heat transfer. Each circuit comprises 2 tube rows and 16 tubes per row. The out-diameter of the finned copper tubes is 8 mm, and the wall thickness 0.68 mm. The longitudinal and transverse tube pitches are 22 mm and 25.4 mm, respectively. The wavy aluminum fins are 0.16 mm thick with 2.12 mm spacing. The whole gas cooler has a length of 1600 mm and a width of 812.8 mm.

Six WL1 90 full-cone nozzles mentioned in Section 2.2 are assumed to be installed 300 mm upstream of the gas cooler. The nozzles are arranged in two rows, with three nozzles in each row. The spacing between adjacent nozzles is 560 mm in the longitudinal (gas-cooler length) direction and 351 mm in the transverse (width) direction. This configuration promotes droplet dispersion and thermal equilibration before entering the gas cooler, ensuring strong agreement with the test conditions to obtain Equation (17).

The $CO_2$ mass flow rate is 0.04 kg/s, air velocity 2.0 m/s, inlet pressure 1.0 bar, and intermediate pressure 32 bar. The evaporating temperature of $CO_2$ in the evaporator is −8 °C, and the superheat at the outlet is 8 K. The air temperature varies in the range of 30 °C to 40 °C. The ratio $R_{wat-air}$ is deliberately limited to $\leq$0.1, with low-flow-rate full-cone nozzles producing a well-coupled homogeneous mist.

## 3. Results and Discussion

### *3.1. Spray-Cooled Gas Cooler Model Validation*

Accurate modeling of the gas cooler is critical for reliable performance predictions in trans-critical $CO_2$ refrigeration systems, particularly due to the highly non-linear thermophysical behavior of $CO_2$ near its critical point and the complex coupled heat and mass transfer occurring during air/water spray cooling. To evaluate the validity and robustness of the detailed spray-cooled gas cooler model developed in this study, the simulation results were compared against experimental measurements obtained from a finned-tube $CO_2$ gas cooler equipped with the low-flow-rate full-cone nozzle, as described in Section 2.2. Validation experiments were conducted over air velocities of 0.7 m/s to 1.4 m/s, with three constant spray-water mass flow rates (12 g/s, 14 g/s, and 16 g/s) for each air velocity. Ambient air was maintained at 30 °C, and the relative humidity was controlled at 50% by a central heating and air conditioning unit. Spray-water was controlled at 20 °C by another heating and cooling unit. The $CO_2$ mass flow rate was 37 g/s, with inlet temperature and pressure of approximately 87 °C and 74 bar, respectively.

Figure 6 compares predicted and measured heat transfer rates and shows agreement within ±15%. Given the strong property variations, local pressure fluctuations, compressibility effects, and two-phase-like behaviors near the pseudo-critical region, which introduce inherent variability that makes experimental measurement challenging, these deviations are consistent with prior literature and acceptable for engineering analysis, indicating the model reliably captures dominant heat-transfer behavior. Figure 7a presents the comparison of $CO_2$-side pressure drop, with the model underpredicting measurements by 7–16%. This difference is mainly due to experimental uncertainties and limitations of classical friction-factor correlation under supercritical $CO_2$ conditions. Figure 7b compares the pressure drop of the air/water mist flow and shows agreement within ±15% for all test cases. Overall, the comparisons confirm the model's capability to accurately predict both heat transfer and pressure-drop characteristics of finned-tube gas coolers under spray-cooling conditions.

### *3.2. Pressure–Enthalpy and Temperature–Entropy Diagrams*

The thermodynamic performance of the trans-critical $CO_2$ refrigeration system is demonstrated by the pressure–enthalpy (*p*–*h*) and temperature–entropy (*T*–*s*) diagrams. The *p*–*h* diagram highlights energy distribution and pressure levels, while the *T*–*s* diagram emphasizes irreversibility and heat transfer characteristics. Figure 8 presents the *p*–*h* and *T*–*s* diagrams under two operating conditions, dry-air cooling ($R_{wat-air} = 0$) and spray cooling ($R_{wat-air} = 0.05$), corresponding to different gas cooler heat rejection methods and resulting in distinct thermodynamic paths.

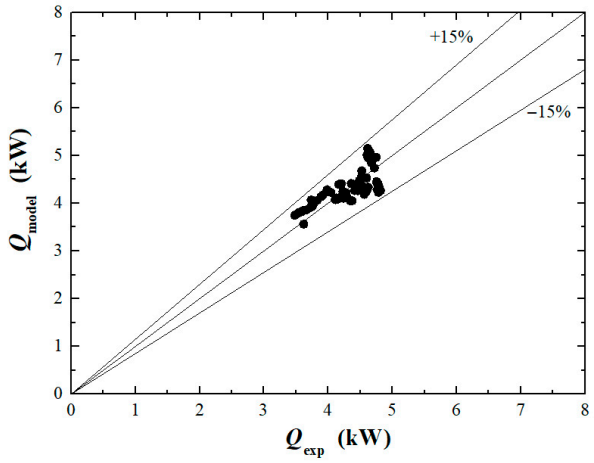


**Figure 6.** Comparison of heat transfer rate between model predictions and experimental results.

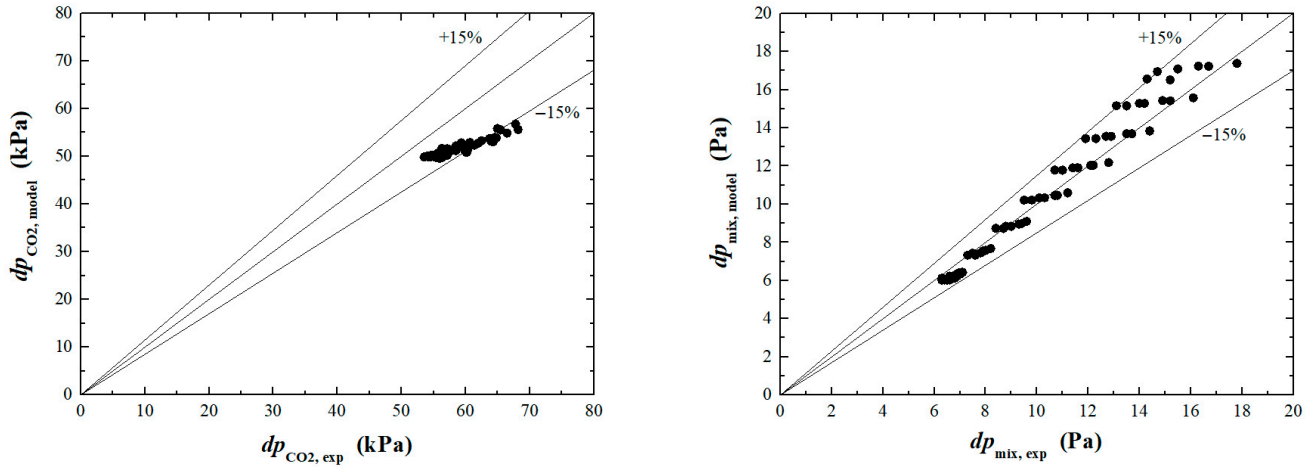


**Figure 7.** Comparison of pressure drops between model predictions and experimental results. (**a**) pressure drop on $CO_2$ side and (**b**) pressure drop on air/water mixture side.

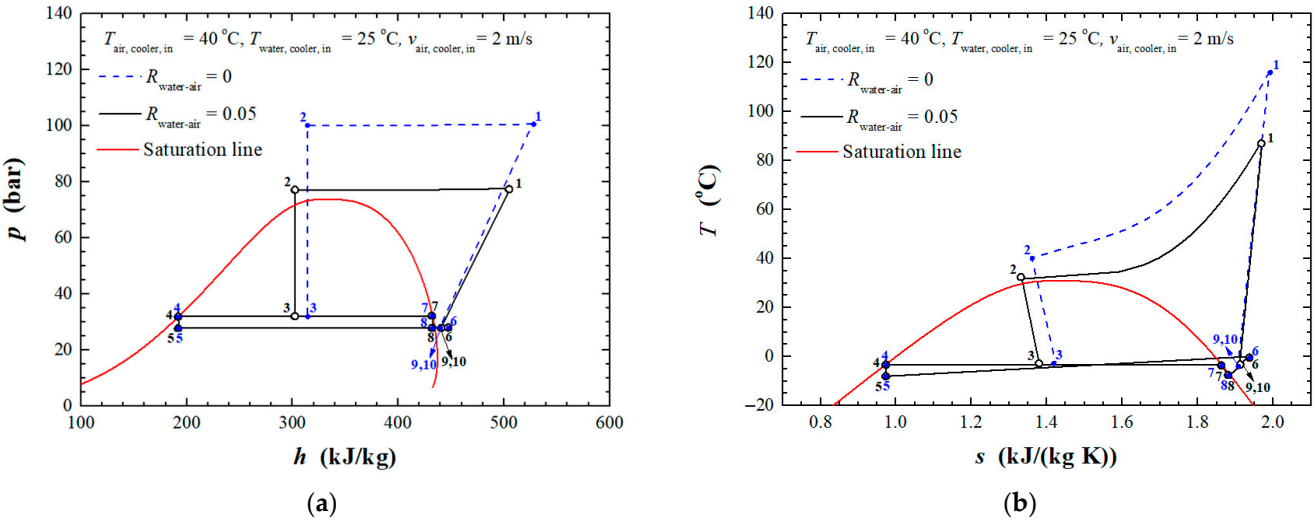


**Figure 8.** Thermodynamic performance comparison. (**a**) *p*–*h* diagram and (**b**) *T*–*s* diagram.

As shown in Figure 8a, both cases follow the canonical trans-critical cycle, comprising compression, gas cooling, expansion, phase separation and evaporation. Significant

differences are observed on the high-pressure side. Spray cooling reduces the compressor discharge pressure and specific enthalpy at point 1 from 100.5 bar and 526.9 kJ/kg to 77.6 bar and 505.8 kJ/kg, respectively. This reduction decreases compressor power consumption from 3.51 kW to 2.62 kW and shifts the compression and gas-cooling processes downward and leftward on the *p*–*h* diagram. The gas cooler outlet enthalpy at point 2 is lower under spray cooling (302.3 kJ/kg vs. 314.3 kJ/kg), bringing the flow closer to the pseudo-critical region and reducing vapor quality after throttling at point 3 (0.423 vs. 0.511). This lower vapor quality leads to increasing $CO_2$ flow entering the evaporator at point 5 (0.0231 kg/s vs. 0.0196 kg/s) and enhancing evaporator cooling capacity between points 5 and 6 (5.86 kW vs. 4.96 kW). The *T*–*s* diagram in Figure 8b further illustrates the impact of spray cooling on system's thermodynamic performance. During the compression process (point 10→1), the spray-cooled case exhibits a smaller entropy increase (0.0612 kJ/(kg K) vs. 0.0835 kJ/(kg K)), indicating reduced irreversibility. Heat rejection (point 1→2) occurs with continuously decreasing temperature and entropy, reflecting the strong variation in $CO_2$ thermophysical properties near the pseudo-critical region. Evaporation (point 5→6) produces a substantial increase in entropy due to phase change and superheating. The comparisons in Figure 8 clearly demonstrate that spray cooling significantly improves system thermodynamic performance by reducing irreversibility, lowering compressor work consumption and increasing evaporator cooling capacity.

### *3.3. Performance of Heat Rejection in Gas Cooler*

Figure 9 shows the variation in gas cooler heat rejection rate and $CO_2$ inlet temperature with increasing spray-water-to-air-mass flow rate ratio ($R_{wat-air}$). The $CO_2$ inlet temperature is primarily determined by the high-side pressure, which depends on the refrigerant thermodynamic state after compression. Increasing $R_{wat-air}$ reduces the gas cooler inlet air temperature, which allows the system to operate at a lower high-side pressure and results in decreased $CO_2$ inlet temperature. The heat rejection rate is governed by both inlet and outlet conditions. Near the pseudo-critical region, small variations in temperature or pressure produce substantial changes in $CO_2$ specific enthalpy, significantly influencing the heat transfer rate. For an air temperature of 40 °C and spray-water temperature of 25 °C, Figure 9a shows an initial slight decrease in heat rejection from 8.51 kW to 7.95 kW as $R_{wat-air}$ increases from 0 to 0.045, due to a modest reduction in high-side pressure and $CO_2$ inlet temperature. Further increasing $R_{wat-air}$ to 0.075 raises the heat rejection to 9.54 kW. Beyond this, the heat rejection rate plateaus, indicating diminishing returns. Correspondingly, as $R_{wat-air}$ increases from 0 to 0.045 and further to 0.075, the $CO_2$ temperature entering the gas cooler decreases from 115.9 °C to 90.5 °C and further to 86.2 °C. These results again confirm that spray cooling significantly improves gas cooler performance and stabilizes system operation under conditions of high ambient temperature.

### *3.4. Performance of Cooling Capacity in Evaporator*

Figure 10 presents the variations in evaporator cooling capacity and $CO_2$ mass flow rate into the evaporator. The $CO_2$ mass flow rate into the evaporator is primarily governed by phase separation process in the liquid receiver, which determines the distribution between liquid and vapor fractions. This separation process is strongly dependent on the thermodynamic state of $CO_2$ at the gas cooler outlet. A reduction in outlet temperature promotes liquid formation, which increases the mass of refrigerant available for expansion into the evaporator. In contrast, a decrease in outlet pressure tends to reduce the liquid fraction, which limits the $CO_2$ mass flow rate into the evaporator. For an air temperature of 40 °C and spray-water temperature of 25 °C, the $CO_2$ mass flow rate remains nearly constant at approximately 0.0196 kg/s as $R_{wat-air}$ increase from 0 to 0.015, reflecting the

limited impact of weak evaporative cooling on receiver liquid production. As $R_{wat-air}$ increases from 0.015 to 0.075, the $CO_2$ mass flow rate rises significantly to 0.0274 kg/s, due to the enhanced air-side cooling, reduced gas cooler outlet temperature, and increased liquid $CO_2$ generation. Beyond an $R_{wat-air}$ of 0.075, the $CO_2$ mass flow rate stabilizes, indicating diminishing returns in further liquid production. Because cooling capacity is largely determined by the $CO_2$ mass flow rate into the evaporator, it exhibits a similar trend, increasing from approximately 4.96 kW to 6.95 kW and remaining nearly constant thereafter. These results confirm that spray cooling effectively enhances the refrigerant circulation and system cooling performance under conditions of high ambient temperature.

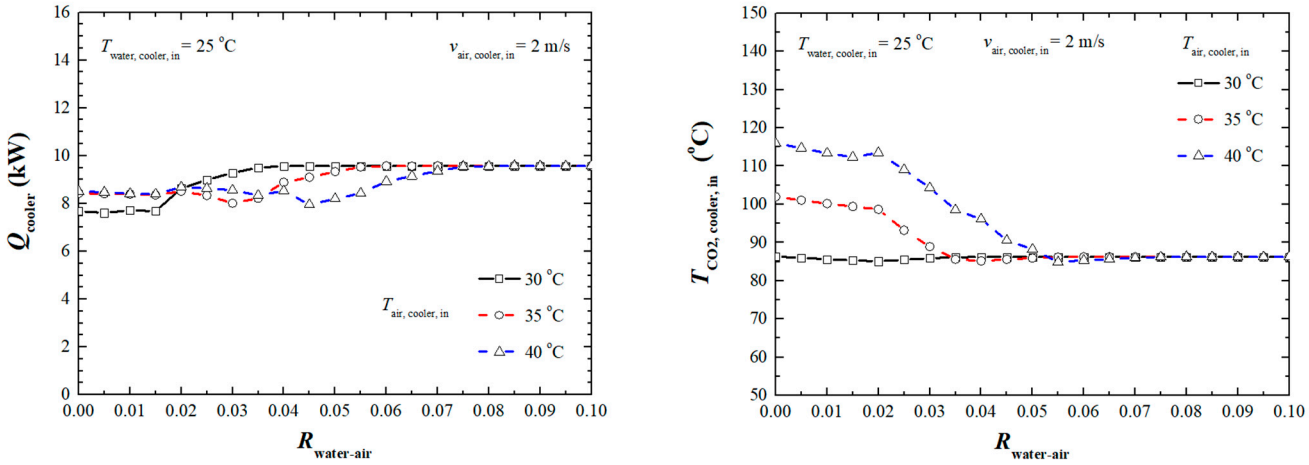


**Figure 9.** Spray-cooled gas cooler performance variation. (**a**) Heat rejection rate and (**b**) $CO_2$ inlet temperature.

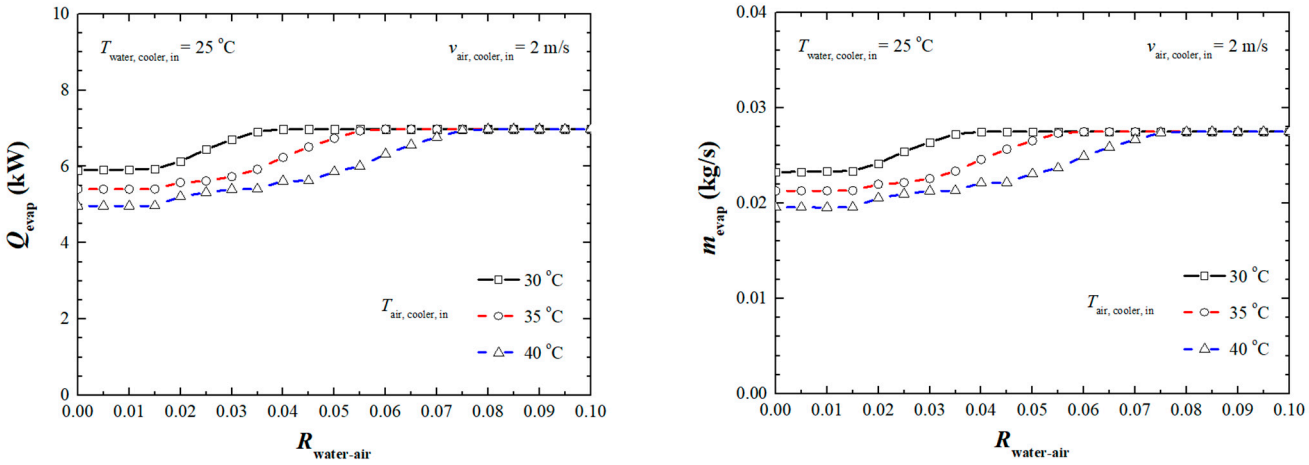


**Figure 10.** Evaporator performance variation. (**a**) Cooling capacity and (**b**) $CO_2$ mass flow rate.

### *3.5. Performance of Compressor Power Consumption*

Figure 11 shows the variation in compressor power consumption and compressor inlet temperature with increasing $R_{wat-air}$. Compressor power is primarily governed by the high-side operating pressure, which determines the compression ratio and corresponding specific work. Therefore, the variation in compressor power closely follows that of the optimal high-side pressure. At an air temperature of 40 °C and spray-water temperature of 25 °C, compressor power decreases from 3.51 kW to 3.42 kW as $R_{wat-air}$ increases from 0 to 0.02, and further decreases to 2.51 kW as $R_{wat-air}$ increases to 0.055. Beyond this

value, additional spray injections produce negligible reductions in power consumption, indicating that once the inlet air temperature approaches the spray-water temperature, further evaporative cooling has minimal influence on the optimal high-side pressure and compression work. The compressor inlet temperature is mainly influenced by phase separation in the liquid receiver, which controls the phase separation between the liquid and vapor fractions of $CO_2$. The vapor leaving the receiver bypasses the evaporative process and mixes with the superheated vapor from the evaporator before entering the compressor. Therefore, the inlet temperature reflects the combined effects of the evaporator outlet conditions and the bypass vapor characteristics. For air temperature of 40 °C and spray-water temperature of 25 °C, at low $R_{wat-air}$ from 0 to 0.02, the $CO_2$ inlet temperature remains nearly constant at approximately −4.89 °C, indicating limited impact on the refrigerant distribution between the liquid and vapor phases. With further increases in $R_{wat-air}$ to 0.075, the inlet temperature rises gradually to −3.07 °C. Further increases in spray ratio result in stabilization of the inlet temperature.

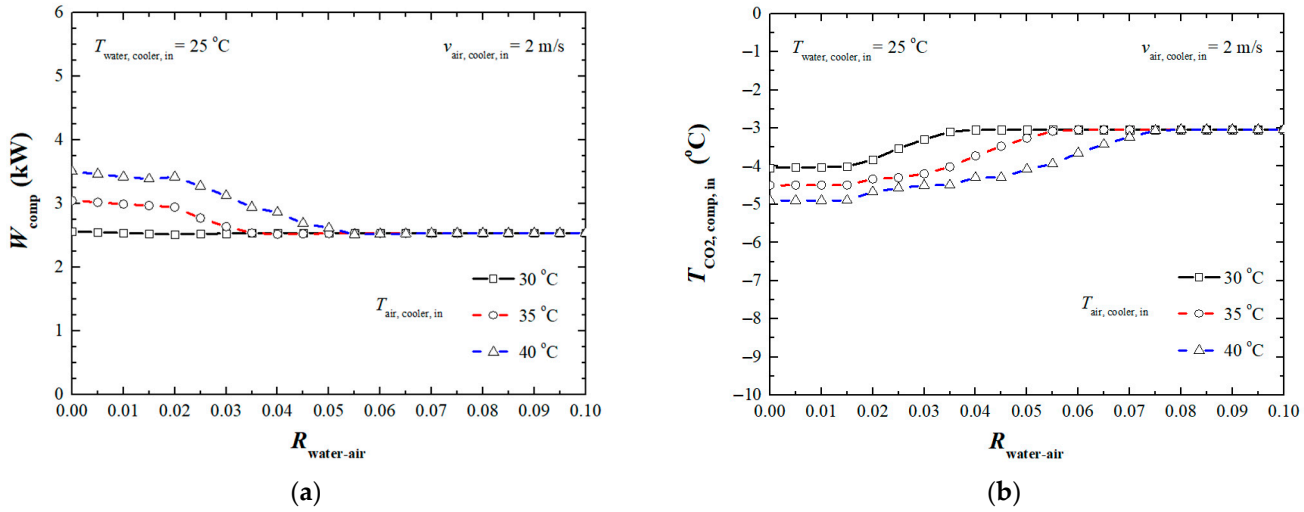


**Figure 11.** Compressor performance variation. (**a**) Power consumption and (**b**) $CO_2$ inlet temperature.

### *3.6. Performance of System COP*

Figure 12a shows the variation in the system *COP* with $R_{wat-air}$ increasing, while Figure 12b presents the corresponding high-side $CO_2$ pressure. Spray cooling significantly reduces the air temperature at the gas cooler inlet, enabling the system to operate at a lower optimal high-side pressure and thereby improving system performance. As shown in Figure 12a, the system *COP* exhibits a three-stage trend with increasing $R_{wat-air}$: a gradual increase, followed by a sharp rise, and finally a plateau. For an air temperature of 40 °C and spray-water temperature of 25 °C, the *COP* increases from 1.42 to 1.53 as $R_{wat-air}$ increases from 0 to 0.02, then rises markedly to 2.74 as $R_{wat-air}$ increases to 0.075, and remains nearly constant thereafter. The initial modest improvement is attributed to limited evaporative cooling, as part of the spray water primarily increases air humidity. The subsequent sharp increase results from a significant reduction in gas cooler inlet temperature, leading to a pronounced decrease in optimal high-side pressure and compressor work. The *COP* plateau indicates diminishing returns once the inlet air temperature approaches the spray-water temperature. The variation in the high-side $CO_2$ pressure exhibits an inverse trend of *COP*. As shown in Figure 12b, the high-side $CO_2$ pressure initially decreases slowly as $R_{wat-air}$ increases from 0 to approximately 0.02 due to the moderate reduction in air temperature, followed by a sharp decline as the enhanced evaporative cooling significantly lowers the gas cooler outlet temperature, and remains nearly constant thereafter. At air temperature of 40 °C and spray-water temperature of 25 °C, the high-side $CO_2$ pressure decreases from

100.5 bar to 98.1 bar as $R_{wat-air}$ increases from 0 to 0.02, further declines to 75.1 bar as $R_{wat-air}$ reaches 0.055, and shows minimal additional change thereafter.

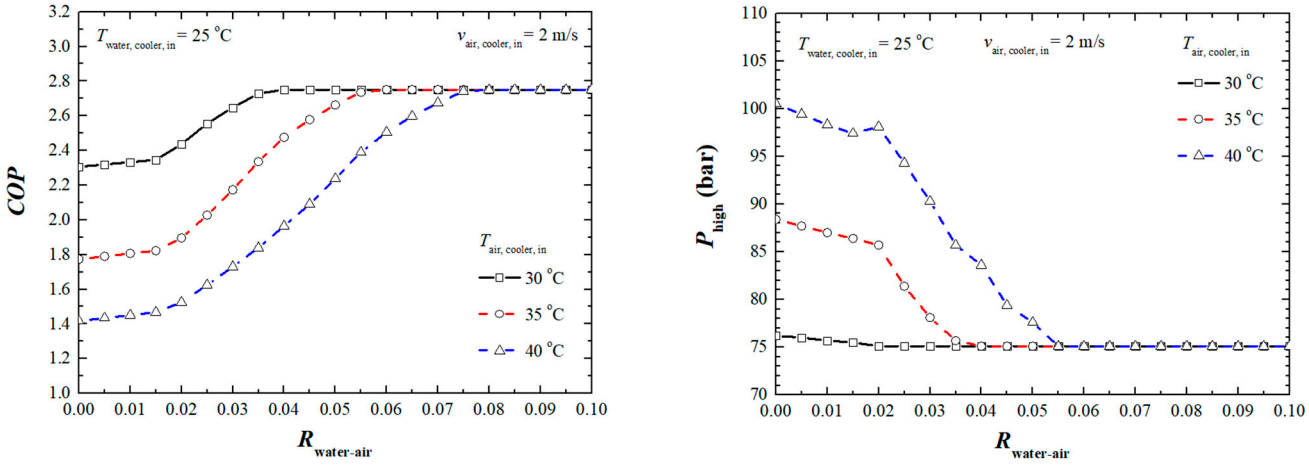


**Figure 12.** System performance variation. (**a**) system *COP* and (**b**) high-side $CO_2$ pressure.

## 4. Conclusions

This study systematically investigated the thermodynamic performance of a trans-critical $CO_2$ refrigeration system integrated with a spray-cooled finned-tube gas cooler, with emphasis on mitigating efficiency degradation under conditions of elevated ambient temperature. A spray-cooled gas cooler model was developed using a homogeneous-mixture approach, treating air and water droplets as a single phase without velocity or temperature differences. After validation against experimental data, the model was integrated into a system-level refrigeration cycle to accurately predict coupled heat and mass transfer processes.

The results demonstrate that spray cooling significantly reduces the $CO_2$ temperatures and operating pressures at both the inlet and outlet of the gas cooler. The heat rejection rate exhibits a slight initial decrease, followed by a substantial increase and eventual stabilization with increasing spray-water-to-air-mass flow rate ratio. Enhanced evaporator performance is primarily attributed to increased liquid $CO_2$ production in the receiver due to lower gas cooler outlet temperatures, which increases the refrigerant mass flow rate through the evaporator and improves cooling capacity.

Compressor power consumption decreases markedly as the optimal high-side pressure and compression ratio are reduced. Consequently, the system *COP* exhibits a three-stage response: a gradual increase at low spray ratios, a pronounced enhancement over an intermediate range, and a plateau beyond a critical value. Under representative high-temperature conditions (air temperature of 40 °C, air velocity of 2 m/s, spray-water temperature of 25 °C), the *COP* increased from 1.53 to 2.74 as the spray-water-to-air-mass flow rate ratio increased from 0.02 to 0.075. The results also indicate that increasing the spray-water-to-air-mass flow rate ratio beyond approximately 0.075 yields negligible additional performance gains, highlighting the existence of an optimal spray operating range.

**Author Contributions:** Conceptualization, L.C. and S.A.T.; methodology, L.C., S.A.T. and K.M.T.; software, L.C. and S.A.T.; formal analysis, L.C.; resources, S.A.T.; data curation, L.C.; writing—original draft preparation, L.C. and K.M.T.; writing—review and editing, L.C., S.A.T. and K.M.T.; project administration, S.A.T.; funding acquisition, S.A.T. and L.C. All authors have read and agreed to the published version of the manuscript.

**Funding:** This research received funding from the Engineering and Physical Sciences Research Council (EPSRC) of the UK under research grants EP/P004636/1—OPTEMIN and EP/V001795/1—SCOTWOHR; from the European Union's Horizon 2020 research and innovation program under grant agreement No. 680599—I-ThERM and Grant Agreement No. 101022831—CO2OLHEAT; and from Brunel Research Culture Seed Fund No. 13157.

**Data Availability Statement:** The original contributions presented in this study are included in the article. Further inquiries can be directed to the corresponding author.

**Conflicts of Interest:** The authors declare no conflicts of interest.

## Nomenclature

| | |
|---|---|
| $A$ | Heat transfer area, $m^2$ |
| $cp$ | Specific heat, J/(kg K) |
| $C$ | Heat capacity rate, W/K |
| $COP$ | Coefficient of performance |
| $D$ | Hydraulic diameter, m; diameter, m |
| $f$ | Friction factor |
| $f1–f7$ | Correlation parameters |
| $F_s$ | Fin spacing, m |
| $G$ | Mass flux, kg/($m^2$ s) |
| GBCV | Gas-bypass control valve |
| GWP | Global warming potential |
| $h$ | Specific enthalpy, J/kg |
| $h_{conv}$ | Heat transfer coefficient, W/($m^2$ K); |
| $i$ | Segment number |
| IPCV | Intermediate-pressure control valve |
| $j$ | Colburn factor |
| $j1–j7$ | Correlation parameters |
| $k$ | Thermal conductivity, W/(m K) |
| $L$ | Length, m |
| LPCV | Low-pressure control valve |
| $m$ | Mass flow rate, kg/s |
| $N$ | Total segment number |
| $NTU$ | Number of transfer units |
| $Nu$ | Nusselt number |
| $P$ | Pressure, Pa; tube pitch, m |
| $Pr$ | Prandtl number |
| $Q$ | Heat transfer rate, W |
| $R$ | Ratio |
| $R_t$ | Thermal resistance, K/W |
| $Re$ | Reynolds number |
| $Re_{Dc}$ | Reynolds number based on tube collar diameter |
| $s$ | Specific entropy, J/(kg K) |
| $S_h$ | Height of slit, m |
| $S_n$ | Slit number in an enhanced zone |
| $S_s$ | Breadth of a slit in airflow direction, m |
| $T$ | Temperature, K |
| $U$ | Overall heat transfer coefficient, W/($m^2$ K) |
| $v$ | Velocity (m/s) |
| $W$ | Work consumption (W) |
| $x$ | Mass quality |
| $\Delta P$ | Pressure drop (Pa) |
| $\Delta T$ | Temperature difference, K |

Greek letters

| | |
|---|---|
| $\rho$ | Density, kg/m$^3$ |
| $\mu$ | Dynamic viscosity, Pa·s |
| $\varepsilon$ | Heat exchanger effectiveness |
| $\eta$ | Efficiency |

Subscripts

| | |
|---|---|
| comp | Compressor |
| evap | Evaporator |
| exp | Experiment |
| ext | External |
| fin | Fin |
| i | Inside |
| in | Inlet |
| is | Isentropic |
| l | Longitudinal |
| max | Maximum |
| min | Minimum |
| mix | Air/water mixture |
| o | Outside |
| out | Outlet |
| t | Transverse |
| total | Total |
| wat | Spray water |

## References


1. Ge, Y.T.; Tassou, S.A. Control optimisation of $CO_2$ cycles for medium temperature retail food refrigeration systems. *Int. J. Refrig.* **2009**, *32*, 1376–1388. [CrossRef]
2. Suamir, I.N.; Tassou, S.A.; Marriott, D. Integration of $CO_2$ refrigeration and trigeneration systems for energy and GHG emission savings in supermarkets. *Int. J. Refrig.* **2012**, *35*, 407–417. [CrossRef]
3. *Natural Refrigerants: State of the Industry*; ATMOsphere Market Report; ATMOsphere: Brussels, Belgium, 2023.
4. *Europe Transcritical $CO_2$ Market*; Report Code BMIRE00029203; Business Market Insights: Pune, India, 2023.
5. *C3S Seasonal Lookback: Summer 2024*; Copernicus: Göttingen, Germany, 2024.
6. Ge, Y.T.; Tassou, S.A. Thermodynamic analysis of transcritical $CO_2$ booster refrigeration systems in supermarket. *Energy Convers. Manag.* **2011**, *52*, 1868–1875. [CrossRef]
7. Kim, J. Spray cooling heat transfer: The state of the art. *Int. J. Heat Fluid Flow* **2007**, *28*, 753–767. [CrossRef]
8. Benther, J.D.; Pelaez-Restrepo, J.D.; Stanley, C.; Rosengarten, G. Heat transfer during multiple droplet impingement and spray cooling: Review and prospects for enhanced surfaces. *Int. J. Heat Mass Transf.* **2021**, *178*, 121587. [CrossRef]
9. Tsamos, K.M.; Ge, Y.T.; Santosa, I.D.M.C.; Tassou, S.A. Experimental investigation of gas cooler/condenser designs and effects on a $CO_2$ booster system. *Appl. Energy* **2017**, *186*, 470–479. [CrossRef]
10. Xiao, L.; Wu, T.; Feng, S.; Du, X.; Yang, L. Experimental study on heat transfer enhancement of wavy finned flat tubes by water spray cooling. *Int. J. Heat Mass Transf.* **2017**, *110*, 383–392. [CrossRef]
11. Dreyer, A.A.; Kriel, D.E.; Erens, P.J. Analysis of spray-cooled finned-tube heat exchangers. *Heat Transf. Eng.* **1992**, *13*, 53–71. [CrossRef]
12. Wataru, N.; Heikichi, K.; Shigeki, H. Heat transfer from tube banks to air/water mist flow. *Int. J. Heat Mass Transf.* **1988**, *31*, 449–460. [CrossRef]
13. Walczyk, H. Enhancement of heat transfer from air-fin coolers with water spray. *Chem. Eng. Process. Process Intensif.* **1993**, *32*, 131–138. [CrossRef]
14. Popli, S.; Hwang, Y.; Radermacher, R. Experimental Investigation of Flat Tube-Louver Fin Heat Exchanger Performance Working as a Cooler in Dry and Wet Conditions. In *ASME International Mechanical Engineering Congress and Exposition*; American Society of Mechanical Engineers: New York, NY, USA, 2012; Volume 45233, pp. 1551–1557. [CrossRef]
15. Chen, C.W.; Yang, C.Y.; Hu, Y.T. Heat transfer enhancement of spray cooling on flat aluminum tube heat exchanger. *Heat Transf. Eng.* **2013**, *34*, 29–36. [CrossRef]
16. Lee, Y.T.; Wen, C.Y.; Chien, L.H.; He, J.; Yang, A.S. Heat transfer of spray falling films over horizontal tubes with counter current airflows in an evaporative condenser. *Int. J. Heat Mass Transf.* **2022**, *183*, 122199. [CrossRef]

17. Hasan, A.; Siren, K. Performance investigation of plain and finned tube evaporatively cooled heat exchangers. *Appl. Therm. Eng.* **2003**, *23*, 325–340. [CrossRef]
18. Wiksten, R.; Assad, M.E.H. Heat and mass transfer analysis of a wavy fin-and-tube heat exchanger under fully and partially wet surface conditions. *Int. J. Therm. Sci.* **2010**, *49*, 349–355. [CrossRef]
19. Ma, H.; Liu, Y.; Xie, Y.; Liu, Y.; Ding, R.; Hou, C.; Lei, Z. Numerical investigation on heat-mass transfer and correlations of humid air-water outside staggered tube bundles. *Int. J. Therm. Sci.* **2022**, *179*, 107632. [CrossRef]
20. Jin, Q.; Yu, Y.; Xia, Y. Experimental study on heat transfer characteristics of spray cooling system with plate-fin heat exchanger. *Exp. Heat Transf.* **2024**, *37*, 767–779. [CrossRef]
21. Bop, I.; Dieng, B.; Mbodji, S.; Bop, G.; Thiam, A. Predicting and optimizing the wet outer surface of water-sprayed finned-tube air-cooled condensers based on purely geometric arguments for inclined sprays: Application on heat transfer enhancement for the cooling of the refrigerant R134a. *Int. J. Thermofluids* **2025**, *29*, 101347. [CrossRef]
22. Zhu, Z.; Li, J.; Liu, J.; Lv, X.; Wang, S.; Liu, B. Simulation and experimental study of heat transfer characteristics of spray-cooled heat exchanger. *Energy Convers. Manag.* **2026**, *351*, 121036. [CrossRef]
23. London, A.L.; Seban, R.A. A generalization of the methods of heat exchanger analysis. *Int. J. Heat Mass Transf.* **1980**, *23*, 5–16. [CrossRef]
24. Park, H.; Roh, J.; cheol Oh, K.; Cho, H.; Kim, J. Modeling and optimization of water mist system for effective air-cooled heat exchangers. *Int. J. Heat Mass Transf.* **2022**, *184*, 122297. [CrossRef]
25. Cao, J.; Ye, M.; Li, H.; Wang, T.; Che, Z. Heat transfer enhancement by mist/air two-phase flow in a high-temperature channel. *Int. J. Heat Mass Transf.* **2022**, *193*, 122966. [CrossRef]
26. Ohkubo, H.; Nishio, S. Study on accurate prediction of heat transfer characteristics of mist cooling: Effects of surface wettability. *JSME Int. J. Ser. 2 Fluids Eng. Heat Transf. Power Combust. Thermophys. Prop.* **1990**, *33*, 326–332. [CrossRef]
27. Gnielinski, V. New equations for heat and mass transfer in turbulent pipe and channel flow. *Int. Chem. Eng.* **1976**, *16*, 359–367.
28. Petukhov, B.S.; Kirillov, P.L. About heat transfer at turbulent fluid flow in tubes. *Therm. Eng.* **1958**, *4*, 63–68.
29. Wang, C.C.; Lee, W.S.; Sheu, W.J. A comparative study of compact enhanced fin-and-tube heat exchangers. *Int. J. Heat Mass Transf.* **2001**, *44*, 3565–3573. [CrossRef]
30. Ge, Y.T.; Tassou, S.A.; Santosa, I.D.; Tsamos, K. Design optimisation of $CO_2$ gas cooler/condenser in a refrigeration system. *Appl. Energy* **2015**, *160*, 973–981. [CrossRef]
31. Santosa, I.M.; Gowreesunker, B.L.; Tassou, S.A.; Tsamos, K.M.; Ge, Y. Investigations into air and refrigerant side heat transfer coefficients of finned-tube $CO_2$ gas coolers. *Int. J. Heat Mass Transf.* **2017**, *107*, 168–180. [CrossRef]